

Chaotic transport in deterministic sine-Gordon soliton ratchets

P. Müller* and F. G. Mertens†

Physikalisches Institut, Universität Bayreuth, D-95440 Bayreuth, Germany

A. R. Bishop

Los Alamos National Laboratory, Los Alamos, New Mexico 87545, USA

(Received 3 March 2008; revised manuscript received 23 September 2008; published 20 January 2009)

We investigate homogeneous and inhomogeneous sine-Gordon ratchet systems in which a temporal symmetry and the spatial symmetry, respectively, are broken. We demonstrate that in the inhomogeneous systems with ac driving the soliton dynamics is chaotic in certain parameter regions, although the soliton motion is unidirectional. This is qualitatively explained by a one-collective-coordinate theory which yields an equation of motion for the soliton that is identical to the equation of motion for a single particle ratchet which is known to exhibit chaotic transport in its underdamped regime. For a quantitative comparison with our simulations we use a two-collective-coordinate (2CC) theory. In contrast to this, homogeneous sine-Gordon ratchets with biharmonic driving, which breaks a temporal shift symmetry, do not exhibit chaos. This is explained by a 2CC theory which yields two ODEs: one is linear, the other one describes a parametrically driven oscillator which does not exhibit chaos. The latter ODE can be solved by a perturbation theory which yields a hierarchy of linear equations that can be solved exactly order by order. The results agree very well with the simulations.

DOI: [10.1103/PhysRevE.79.016207](https://doi.org/10.1103/PhysRevE.79.016207)

PACS number(s): 05.45.Pq, 05.45.Yv, 85.25.Cp, 73.40.Ei

I. INTRODUCTION

In the simplest particle ratchet models a pointlike particle is considered in a periodic potential $U(X)$ that is driven by a periodic force $f(t)$ with zero time average. Under certain conditions related to the breaking of symmetries, unidirectional motion of the particle can take place [1–5].

The dynamics of the particle usually depends strongly on the damping. For strong damping, when the inertial term can be neglected compared to the damping term, the dynamics is rather simple: e.g., in the case of an asymmetric periodic potential $U(X)$ the average velocity $\langle v \rangle = \langle \dot{X}(t) \rangle$ of the particle as a function of the driving amplitude exhibits a “quantized” structure

$$\langle v \rangle = \frac{i}{j} v_{\text{step}} \quad (1)$$

with integers i, j and the step height $v_{\text{step}} = L/T$, where L and T are the periods of the potential and the driving force, respectively. This means that the particle motion is locked to the driver; the particle covers a distance of i periods of the potential during j driving periods [4].

For underdamped particle ratchets the dynamics is much more complicated. In the case of an asymmetric periodic potential and sinusoidal driving $f(t) = A \sin(\omega t)$ the following additional effects show up [6–8]: (1) strong dependence on the initial conditions, (2) appearance of bifurcations and chaotic regimes in plots of $\langle v \rangle$ vs the control parameter A , (3) current reversals, i.e., changes of the sign of $\langle v \rangle$ as A is varied, (4) hysteresis effects in $\langle v \rangle$ varying A .

In the last few years the particle ratchet systems have been generalized to spatially extended nonlinear systems, in which solitons play a similar role as the above point particles [9–15]. In particular, solitons in nonlinear Klein-Gordon systems have been shown to move on the average in one direction, although the driving force has zero time average, if either temporal or spatial symmetry is broken. Both types of ratchet systems can be defined by the equation

$$\phi_{tt} + \beta \phi_t - \phi_{xx} + \frac{\partial \tilde{U}}{\partial \phi} [1 + V(x)] = f(t). \quad (2)$$

Here $\phi(x, t)$ is a scalar field and ϕ_x and ϕ_t are partial derivatives with respect to space and time. We will consider here the sine-Gordon model for which $\tilde{U}(\phi) = 1 - \cos \phi$. The external driving force $f(t)$ has the period T and zero time average.

For $V(x) \equiv 0$ the system is spatially homogeneous. The temporal shift symmetry $f(t) = -f(t + T/2)$ can be broken for instance by using a biharmonic force [16–19]

$$f(t) = \epsilon_1 \sin(\omega t + \delta_1) + \epsilon_2 \sin(m\omega t + \delta_2), \quad (3)$$

where $m > 1$ is an even integer. Here the mechanism of the ratchet effect has been clarified in detail by a collective coordinate (CC) theory [18, 19], which uses the soliton position $X(t)$ and width $l(t)$. Due to the coupling between the translational and internal degrees of freedom, energy is pumped inhomogeneously into the system, generating a unidirectional motion. The breaking of the time shift symmetry gives rise to a resonance mechanism that takes place whenever the width $l(t)$ oscillates with at least one frequency of the external ac force. This ratchet effect has been confirmed by experiments with annular Josephson junctions [20] which can be modeled by sine-Gordon systems; here flux quanta (fluxons) play the role of the solitons. Biharmonic microwaves have been used as the external periodic force.

*patric.mueller@uni-bayreuth.de

†franz.mertens@uni-bayreuth.de

The second way to obtain a soliton ratchet consists in breaking the spatial symmetry of the system. This has been demonstrated very recently by the introduction of strongly localized inhomogeneities $g_i(x)$, which were modeled by δ functions [21,22] or narrow and high box functions [23]. In the case of long Josephson junctions “strongly localized” means that the spatial extent of the inhomogeneities is much smaller than the characteristic length for the system, the Josephson penetration length.

In order to produce a ratchet effect, $V(x)$ in Eq. (2) must consist of periodically repeated cells of length L , where each cell n contains an asymmetric array of inhomogeneities which are placed at positions x_i within the cell, i.e.,

$$V(x) = \sum_n \sum_i g_i(x - x_i - nL). \quad (4)$$

In most studies a single ac force

$$f(t) = A \sin(\omega t + \delta_0) \quad (5)$$

has been used [21–23]. The case of two ac forces with different frequencies [24] will not be considered here. The aim of this paper is to explain why the above two types of systems, homogeneous and inhomogeneous, exhibit a soliton dynamics that qualitatively differs very much in at least two important aspects.

(1) The homogeneous systems are very robust against chaos: In Ref. [19] very small damping coefficients ($0.01 \leq \beta \leq 0.5$) were chosen and the driving frequency ω was rather large (0.1 or 0.25), nevertheless no chaos showed up. The same holds for even larger frequencies (Sec. V). In contrast to this, the inhomogeneous sine-Gordon ratchets exhibit chaos if the driving frequency ω is high enough and if both the damping β and the driving amplitude A are relatively small (Sec. II). Moreover, chaotic transport is possible unexpectedly in certain small parameter regions; e.g., for relatively large damping ($\beta=0.8-0.9$) plus strong driving [$A=O(1)$]. This will be discussed in detail in Sec. II.

(2) In the homogeneous systems the average soliton velocity $\langle v \rangle$ is a smooth and differentiable function of the parameters of the model, e.g., amplitudes, frequencies, and phases in the biharmonic driving force (3). In contrast to this, in the inhomogeneous systems $\langle v \rangle$ exhibits a staircase structure.

We will first investigate the inhomogeneous sine-Gordon ratchets. In Sec. II we present a set of typical soliton trajectories $X(t)$ which exhibit regular or chaotic transport; then we show in which parameter regions chaotic transport occurs. In Sec. III a 1CC theory demonstrates that the soliton motion can be described as the motion of a pointlike particle in an effective potential which is periodic and asymmetric. For such a particle ratchet model chaotic transport is well known [6–8]. For a detailed comparison with the simulations we use a 2CC theory in which the soliton width $l(t)$ is the second collective coordinate.

The ratchet mechanism in homogeneous sine-Gordon models with biharmonic driving cannot be explained by a 1CC theory. In Ref. [17] it was argued that the observed rectification arises from the excitation of internal kink modes and their interaction with the translational kink motion. This

conjecture was confirmed by a 2CC theory [18,19] which reveals a resonance phenomenon, see below Eq. (3). Moreover, this theory suggests that no chaos occurs in these systems (Secs. IV and V): The two ODEs for the soliton position $X(t)$ and width $l(t)$ can be decoupled by the introduction of the soliton momentum $P(t)$ which obeys a linear equation. The remaining ODE for $l(t)$ represents a nonlinear oscillator which is driven parametrically by the harmonics contained in $P^2(t)$ and does not exhibit chaos. The comparison with the simulation results is made in Sec. V, and the conclusions are presented in Sec. VI.

II. INHOMOGENEOUS RATCHETS: SIMULATIONS

Strongly localized inhomogeneities, the g_i in Eq. (4), have been modeled by δ functions [21,22] or by narrow and high box functions [23]. We choose here the boxes because they are more realistic and can be implemented more easily in our simulation program. Moreover, the number, shape and positions x_i of the boxes within the periodically repeated cells have been optimized in Ref. [23], in the sense that the average soliton velocity $\langle v \rangle$ and thus the current is as high as possible. For strong damping ($\beta=1$) and low driving frequency ($\omega=0.015$ or 0.05) the optimal array consists of two boxes with equal halfwidth ($b=0.1$) and equal height, but with opposite signs ($h_1=25$, $h_2=-h_1$). The positions x_1 and x_2 are chosen such that the boxes touch each other, but do not overlap, i.e., $x_2 - x_1 = 2b$. The array length is $L=4, 6$, or 8 and in this range L has little influence on $\langle v \rangle$.

We remark that the above two types of inhomogeneities, having a positive or a negative sign, have already been used in experiments with long Josephson junctions: so-called “microresistors” (critical current J_c decreased) and “microshorts” (J_c increased) [25]. Plots of $\langle v \rangle$ vs the driving amplitude A exhibit a staircase structure similar to the case of particle ratchets: $j=1$ in Eq. (1) and with increasing amplitude i first increases ($i=1, 2, 3, \dots, i_{\max}$), then decreases. But before $i=0$ can be reached the system enters a regime in which kink-antikink pairs appear spontaneously and spoil the ratchet effect. For the above parameters the maximum of $\langle v \rangle$ is on the order of 0.15 (in units of the critical velocity $v_c = 1$ of the unperturbed sine-Gordon model). The value 0.15 is quite high, bearing in mind that $\langle v \rangle$ is an average which includes soliton velocities $v(t)$ not far from the critical velocity.

The above results were obtained for strong damping ($\beta=1$) and low driving frequency. In this paper we are interested in chaotic transport and therefore we reduce the damping and increase the driving frequency but do not change the parameters of the inhomogeneities. We numerically solve Eq. (2) by using a fourth-order Runge-Kutta scheme with step sizes $\Delta t=0.01$ and $\Delta x=0.05$.

In Fig. 1 we present some examples from a typical set of soliton trajectories $X(t)$ with $\beta=0.4$ and a relatively high driving frequency ($\omega=0.38$), varying the driving amplitude A . For $A < A_{\min} \approx 0.49$ there is no ratchet effect, for $0.49 \leq A_{\min} \leq 0.57$ we get unidirectional transport with n -periodic solutions, where n decreases as A increases ($n=22, 5, 3, 2$ for $A=0.49, 0.5, 0.52, 0.57$, respectively). Here the average ve-

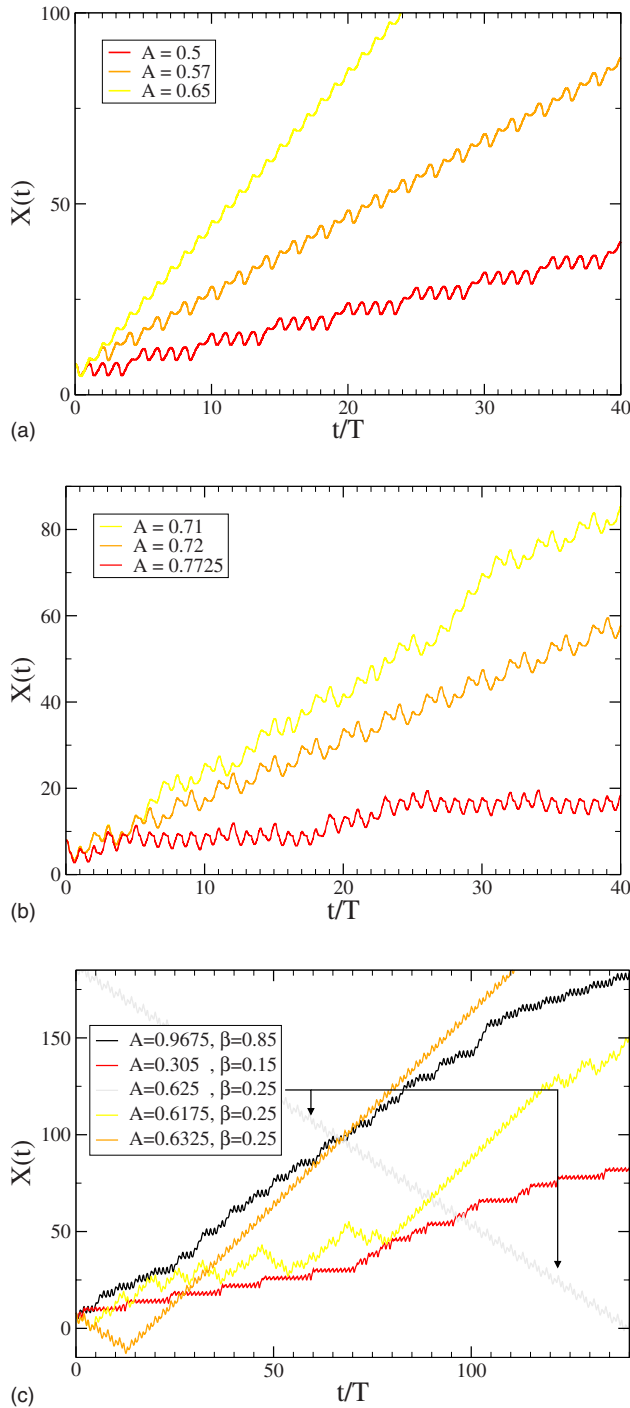


FIG. 1. (Color online) (a), (b) Simulation results for a ratchet with box inhomogeneities of period $L=4$ (see text), for damping $\beta=0.4$. The soliton position $X(t)$ is plotted vs time in units of the period $T=2\pi/\omega$ of ac driving with frequency $\omega=0.38$. (a) n -periodic regular trajectories with $n=5, 3,$ and 1 . (b) Chaotic, five-periodic, and chaotic trajectories for $A=0.71, 0.72,$ and 0.7725 , respectively. (c) Some special trajectories on a larger time scale, see text.

locity $\langle v \rangle$ increases according to Eq. (1) with $i=1$ and $j=n$. Then a broad A interval $[0.58, 0.7]$ with one-periodic solutions appears in which $\langle v \rangle$ has its maximum value L/T . Above this interval there is an irregular sequence of chaotic

and n -periodic trajectories [Fig. 1(b)]. The intermittency in the chaotic soliton trajectories is not strongly pronounced, compared to particle ratchet models where long times with regular behavior are interrupted by short bursts with irregular behavior [7].

Figure 2(a) summarizes which types of soliton trajectories (no transport, regular or chaotic transport) occur in the region $0.02 \leq \beta \leq 1, 0 \leq A \leq 1$. We distinguish between the different types of trajectories by using dynamical systems methods from “symbolic dynamics” (Appendix). For small damping and strong driving (dark gray regions in Fig. 2) no definite trajectories can be determined, because the soliton is strongly deformed such that its position is no longer defined (Appendix). The soliton can also develop into a complicated structure with additional kink-antikink pairs.

As expected, the transport is nearly always chaotic for small damping (e.g., $\beta=0.1$), while it is nearly always regular for large damping (e.g., $\beta=0.7$). However, somewhat surprising is the fact that chaos also occurs in a small stripe with large damping ($\beta=0.8-0.9$) and strong driving ($A=0.9-1.0$). A typical trajectory from this stripe is shown in Fig. 1(c), together with an example for the opposite case: small damping ($\beta=0.15$) and weak driving ($A=0.305$).

Figure 2(c) displays the average soliton velocities for the same parameter region as in Fig. 2(a). The average is taken over 30 periods T , after having waited a sufficiently long time (ten periods) until transients have elapsed. The sharp lines between the different gray-scale-values appear due to the “quantization” of the velocity according to Eq. (1). This equation only holds for regular transport, therefore there are no sharp lines at the boundaries to regions with chaotic transport.

An interesting detail in Fig. 2(c) ($\beta \approx 0.25, A \approx 0.625$) are the small black regions in which $\langle v \rangle$ is negative (current reversal). Figure 1(c) displays three trajectories from a scan for $\beta=0.25$ through the largest black region. We mention that current reversals were already observed in a sine-Gordon system with asymmetric field potential, for similar values of driving amplitude and damping [26]. The phenomenon was attributed to the influence of phonon modes, because a CC theory cannot describe it. In fact, the situation is quite similar for our inhomogeneous sine-Gordon system, because the CC-theory in Sec. III also does not yield current reversals, see Fig. 5(b). When the driving frequency is reduced, starting from $\omega=0.38$, the white chaotic regions in Fig. 2(a) shrink more and more and eventually vanish.

In Fig. 3 we present $\langle v \rangle$ as a function of ω , for fixed A and β . Here $\langle v \rangle$ is averaged over 30 single, successive driving periods, i.e., up to 30 different points can be seen for each ω . For small ω we observe unidirectional transport with one-periodic solutions. For larger ω there are either n -periodic or chaotic trajectories. In the hatched regions for even larger ω there are no definite trajectories [see the dark gray regions in Figs. 2(a) and 2(b)]. And above that region there is no unidirectional transport.

Finally we demonstrate in Fig. 4 that bifurcations, regions with n -periodic solutions and chaotic regions, appear in a Poincaré plot with the control parameter A . Here the soliton velocity $\dot{X}(t)$ is plotted for 30 successive time values $t, t+T, t+2T,$ etc.

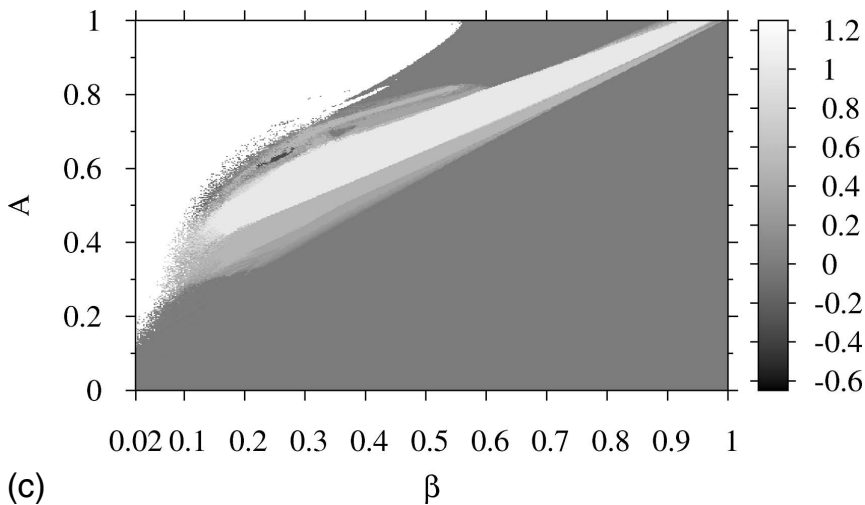
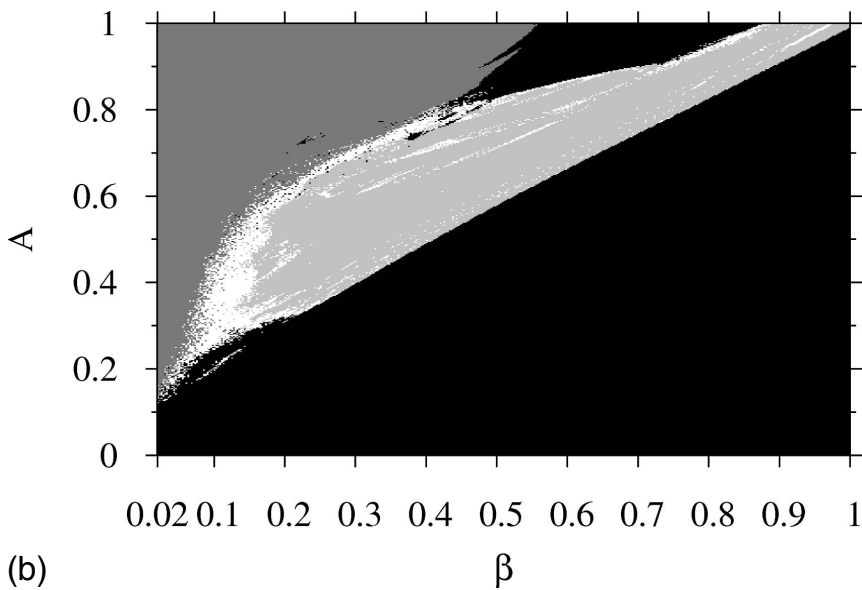
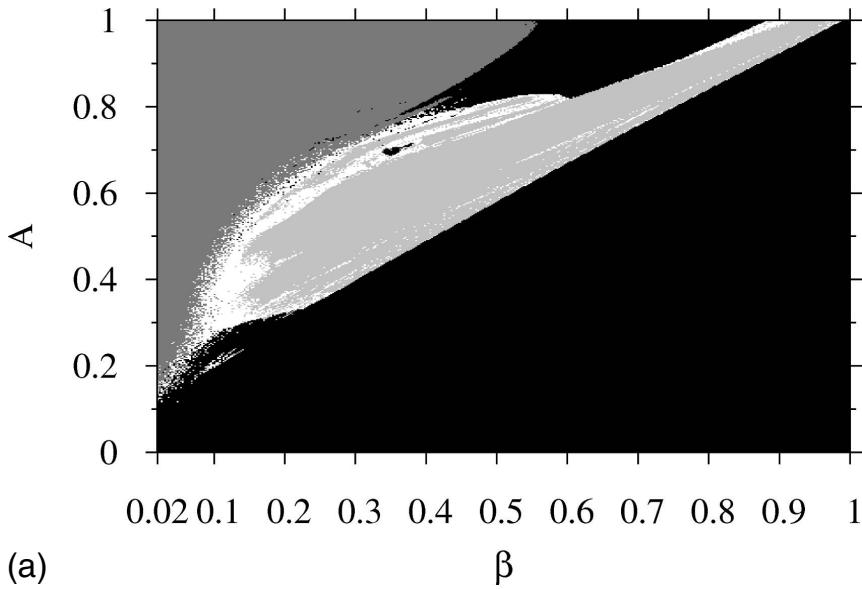


FIG. 2. Simulation results for the same inhomogeneous ratchet as in Fig. 1, with driving frequency $\omega=0.38$. (a) Type of transport as a function of driving amplitude A and damping β ; black: no transport, light gray: regular transport, white: chaotic transport, dark gray: no definite trajectories (see text). (c) Mean soliton velocity $\langle v \rangle$, in units of $v_{\text{step}}=L/T$. In the black regions $\langle v \rangle$ is negative (current reversal). White region: No definite trajectories [dark gray regions in (a)]. (b) The same as in (a) but now with additional weak subharmonic driving ($A_{\text{sub}}=0.02$, $\omega_{\text{sub}}=\omega/2$).

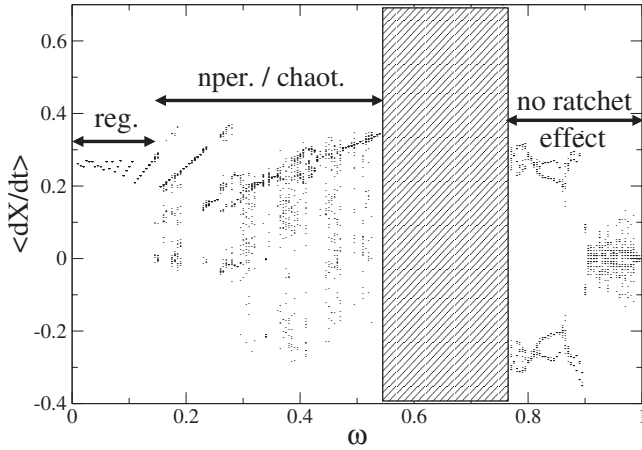


FIG. 3. Soliton velocity averaged over 30 single successive periods (after having waited for 20 periods), as a function of the driving frequency ω , for fixed driving amplitude $A=0.5$ and damping $\beta=0.15$. The different regions are discussed in the text.

Another interesting point is the stabilization of the soliton dynamics by weak periodic signals. For particle ratchets it is well known that chaos can be suppressed applying weak subharmonic signals [27]. To check whether this also holds for the soliton ratchet studied here, we have run simulations with an additional weak subharmonic driving force $f(t) \rightarrow A \sin(\omega t + \delta_0) + A_{\text{sub}} \sin(\omega_{\text{sub}} t)$. Figure 2(b) shows the result for $\omega_{\text{sub}} = \omega/2 = 0.19$, $A_{\text{sub}} = 0.02$, and $\delta_0 = 0.0$. As one can see, some chaotic (white) regions disappear. The stabilizing effect of weak subharmonic signals as shown in Ref. [27] for particle ratchets hence also works for soliton ratchets.

III. INHOMOGENEOUS RATCHETS: THEORY

First we demonstrate that a simple theory with only one collective coordinate (ICC theory) is sufficient to understand why and roughly when chaos appears in the inhomogeneous

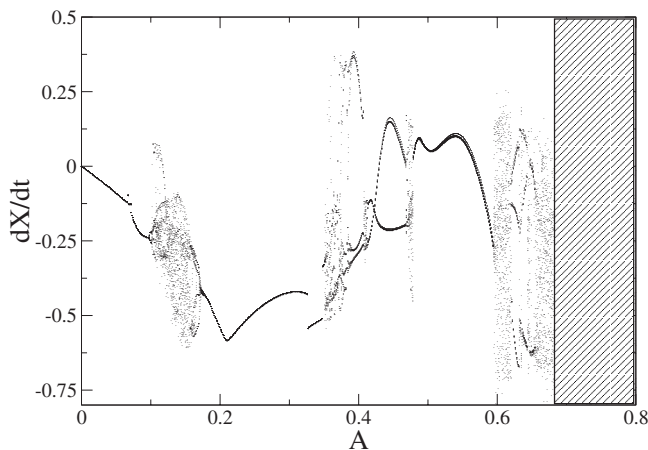


FIG. 4. Soliton velocity for 30 successive time values $t, t+T, t+2T, \dots$ (after having waited for 20 periods), varying the driving amplitude A . The figure shows simulation results for the same inhomogeneous ratchet as in Fig. 1. Model parameters are $\omega=0.38$ and $\beta=0.25$.

systems, in contrast to the homogeneous systems for which a ICC theory does not work [17,18,28]. In a second step we shortly review the 2CC theory [21–23] which will then be used to make a quantitative comparison with the simulation results of Sec. II.

The one-soliton solution of the unperturbed sine-Gordon equation is used to make the following ansatz:

$$\phi(x,t) = 4 \arctan \left[\gamma \frac{x - X(t)}{l_0} \right], \quad (6)$$

with the soliton position $X(t)$, $\gamma = 1/\sqrt{1-\dot{X}^2}$ and the soliton rest width $l_0=1$.

Using a procedure first proposed in Ref. [29] the following equation of motion for the soliton is obtained [22]:

$$\gamma^3 M_0 \ddot{X} + \beta \gamma M_0 \dot{X} = -qf(t) - \frac{\partial U}{\partial X}. \quad (7)$$

Here $M_0=8$ is the soliton rest mass, $\gamma^3 M_0$ is the so-called longitudinal relativistic mass, $q=2\pi$ is the topological charge of the soliton, $f(t)=A \sin(\omega t)$, and $-\partial U/\partial X$ is a force due to an effective potential

$$U = \int_{-\infty}^{\infty} dx \, 2 \operatorname{sech}^2[\gamma(x-X)] V(x). \quad (8)$$

As $V(x)$ consists of periods of length L , where each period contains an asymmetric array of the inhomogeneities g_i [Eq. (4)], the effective potential $U(X)$ is also periodic with period L and is asymmetric.

The integral in Eq. (8) can be evaluated analytically for δ functions or box inhomogeneities [22,23]. But here we do not need the results, because for this paper the only important fact is that Eq. (7) has the same form as the deterministic equation of motion for a periodically driven pointlike particle in an asymmetric periodic potential, as discussed at the beginning of the Introduction. (However, in most of the literature on particle ratchets the nonrelativistic limit was considered.)

Thus we can conclude that in the overdamped regime ($\beta \gg \omega$), when the inertial term can be neglected compared to the damping term, the solitons always have regular trajectories and plots of $\langle v \rangle$ vs A exhibit the staircase structure of Eq. (1). This is confirmed by our simulations.

If β is on the same order as ω or even much smaller (underdamped regime), we expect the four additional effects listed in Sec. I for particle ratchets. In particular we are interested in chaotic transport and current reversals when β is reduced and ω is increased (compared to the parameters in Refs. [21–23]: $\beta=1$, $\omega=0.015, 0.05, 0.1$).

However, for larger ω the ICC theory does not agree so well with the simulations. For example, for $\omega=0.1$ it predicted two so-called “windows” (regions of A in which $\langle v \rangle \neq 0$) while the simulation yielded only one window [21].

Therefore we need to improve the ICC theory by introducing a second collective coordinate, namely, the soliton width $l(t)$. We use the so-called Rice ansatz [30] which was originally made in order to calculate approximately the internal mode of solitons in nonlinear Klein-Gordon models.

Later the Rice ansatz was used to predict an unexpected resonance in the ac-driven ϕ^4 model [31,32] and recently it was applied to nonlinear Klein-Gordon ratchets [18,19,21,22]. For the sine-Gordon model the ansatz reads

$$\phi(x,t) = 4 \arctan \left[\exp \left(\frac{x - X(t)}{l(t)} \right) \right] \quad (9)$$

and in the case of inhomogeneous ratchet systems the 2CC theory yields the two coupled ODEs [22]

$$M_0 l_0 \frac{\ddot{X}}{l} + \beta M_0 l_0 \frac{\dot{X}}{l} - M_0 l_0 \frac{\dot{X} \dot{l}}{l^2} = F^{\text{ac}} + F^{\text{inh}}, \quad (10)$$

$$\alpha M_0 l_0 \frac{\ddot{l}}{l} + \beta \alpha M_0 l_0 \frac{\dot{l}}{l} + M_0 l_0 \frac{\dot{X}^2}{l^2} = K^{\text{int}} + K^{\text{inh}}, \quad (11)$$

where $\alpha = \pi^2/12$, $M_0 = 8$, and $l_0 = 1$ is the soliton rest width

$$F^{\text{ac}} = \int_{-\infty}^{\infty} dx f(t) \frac{\partial \phi}{\partial X} = -qf(t) \quad (12)$$

with the topological charge $q = 2\pi$ is an effective driving force and

$$K^{\text{int}} = - \frac{\partial E}{\partial l} \quad (13)$$

is a force which arises from the soliton energy

$$E(\dot{X}, l, \dot{l}) = \frac{1}{2} \frac{l_0}{l} M_0 \dot{X}^2 + \frac{1}{2} \frac{l_0}{l} \alpha M_0 \dot{l}^2 + \frac{1}{2} M_0 \left(\frac{l_0}{l} + \frac{l}{l_0} \right), \quad (14)$$

including internal energy due to width oscillations. There are two forces that appear due to the potential $V(x)$ in Eq. (2):

$$F^{\text{inh}} = - \int_{-\infty}^{\infty} dx \frac{\partial \tilde{U}}{\partial \phi} \frac{\partial \phi}{\partial X} V(x) = - \int_{-\infty}^{\infty} dx \frac{\partial \tilde{U}}{\partial X} V(x) := - \frac{\partial U}{\partial X}, \quad (15)$$

$$K^{\text{inh}} = - \int_{-\infty}^{\infty} dx \frac{\partial \tilde{U}}{\partial \phi} \frac{\partial \phi}{\partial l} V(x) = - \int_{-\infty}^{\infty} dx \frac{\partial \tilde{U}}{\partial l} V(x) := - \frac{\partial U}{\partial l}. \quad (16)$$

with the effective potential

$$U(X, l) = \int_{-\infty}^{\infty} dx \tilde{U}(\phi) V(x). \quad (17)$$

$\tilde{U}(\phi) = 1 - \cos \phi$ can be evaluated for the ansatz (9) which yields [23]

$$U(X, l) = \int_{-\infty}^{\infty} dx 2 \operatorname{sech}^2 \frac{x - X}{l} V(x), \quad (18)$$

where $V(x)$ consists of strongly localized inhomogeneities g_i as defined in Eq. (4).

In the following we use box functions as inhomogeneities, because for this choice the integral 18 can be evaluated analytically [23],

$$U(X, l) = \sum_n \sum_i 2h_i l \sinh \frac{2b_i}{l} \operatorname{sech} \frac{Z_+}{l} \operatorname{sech} \frac{Z_-}{l}, \quad (19)$$

with $Z_{\pm} = X - x_i - nL \pm b_i$. Here h_i and b_i are the height and half width of the box i at position x_i within cell n . All cells have length L and are repeated periodically. We use the same array of two adjacent boxes with opposite signs as in our simulations in Sec. II: $b_1 = b_2 = 0.1$, $h_1 = 25$, $h_2 = -h_1$, $x_2 - x_1 = 0.2$.

The two ODEs [Eqs. (10) and (11)] can easily be solved numerically.

Figure 5(a), which displays the different types of transport for the A - β plane, agrees quite well with the corresponding simulation results in Fig. 2(a). There are, however, some quantitative differences. The most important one is that for $A \gtrsim 0.3$ the roughly diagonal line which separates the black no-ratchet regime from the light gray (regular) and white (chaotic) ratchet regimes is tilted to the right in the simulations, compared to the theory. This means that the slope of the line is smaller than the theory predicts. The explanation is that in the sine-Gordon equation there are many more degrees of freedom than in 2CC theory. They represent a kind of noise bath which means that the damping is effectively increased. For example, the point $\beta = 0.57$, $A = 0.7$ on the diagonal line is shifted to the right to $\beta = 0.63$, $A = 0.7$ in the simulations. This effect is stronger the higher the amplitude A . Another important difference is that in the simulations the white chaotic regions are considerably smaller than in the theory. At first glance this is surprising because one would expect less chaos in the two ODEs of the theory than in the sine-Gordon equation which is a PDE. But we are dealing here only with chaotic transport of solitons, not with chaos in general, and solitons are nonlinear coherent excitations which are very robust, both in an environment with deterministic chaos [33] and in the presence of thermal noise [34].

The distribution of the mean soliton velocities $\langle v \rangle$ in the A - β plane is seen in Fig. 5(b) and has to be compared with Fig. 2(c). As there are much larger chaotic regions in the theory than in the simulations, the ‘‘quantization’’ of $\langle v \rangle$ is much less pronounced here. Another important difference is that there are no regions with current reversals, in contrast to the appearance of the small black regions in Fig. 2(c).

IV. HOMOGENEOUS RATCHETS: THEORY

We consider the sine-Gordon Eq. (2) with $V(x) \equiv 0$ and the biharmonic driving force in Eq. (3), which breaks a temporal symmetry. In this case a 2CC theory is needed, as has already been explained below Eq. (3). The resulting ODEs (see Refs. [18,19]) for the soliton position $X(t)$ and width $l(t)$ are a special case of Eqs. (10) and (11) in which the inhomogeneous forces F^{inh} and K^{inh} in Eqs. (15) and (16) now vanish identically. Thereby the character of the equations is changed completely: The introduction of the soliton momentum

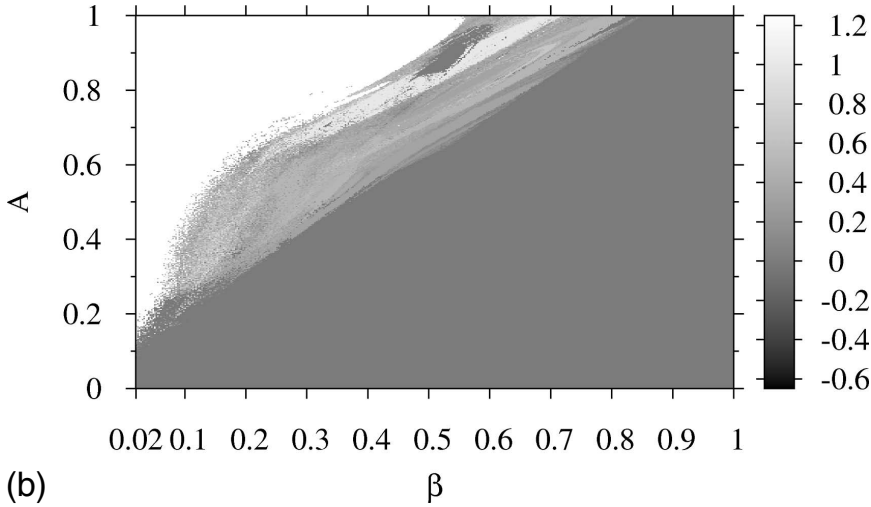
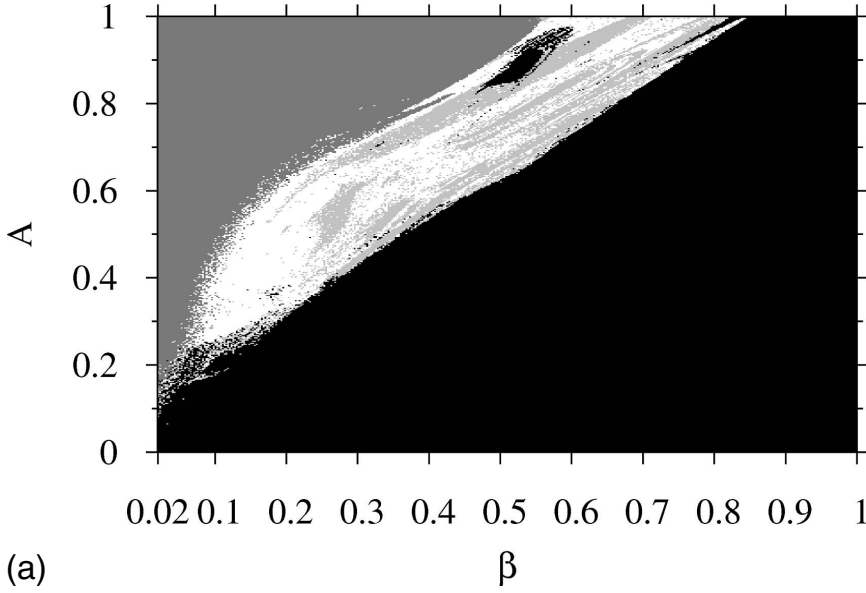


FIG. 5. Results from 2CC theory for inhomogeneous ratchets, to be compared with the simulation results in Fig 2. (a) Type of transport. (b) Mean soliton velocity in units of $v_{\text{step}}=L/T$.

$$P(t) = M_0 l_0 \dot{X}/l \quad (20)$$

allows transformation of the ODE for $X(t)$ into a linear equation for $P(t)$ which is decoupled from the ODE for $l(t)$

$$\dot{P} + \beta P = -qf(t). \quad (21)$$

Thus $P(t)$ cannot exhibit chaos. Possibly this holds only for the theory, not for the simulations, since the Rice ansatz (9) is an approximation. However, Eq. (21) can be shown to be exact [35], by using the field-theoretic definition of the momentum

$$P(t) = - \int_{-\infty}^{\infty} dx \phi_t \phi_x. \quad (22)$$

The solution of Eq. (21), after transients have elapsed and become negligible ($t \gg 1/\beta$), has a similar biharmonic structure as the driving force (3). Both harmonic terms in $P(t)$ have an additional phase shift and the amplitudes are functions of the parameters β , ϵ_1 , ϵ_2 , ω , and m .

The ODE for $l(t)$ reads, after the substitution (20),

$$l^2 - 2l\ddot{l} - 2\beta l\dot{l} = \Omega_R^2 l^2 \left(1 + \frac{P^2}{M_0^2} \right) - \frac{1}{\alpha}, \quad (23)$$

where $\Omega_R = 1/(\sqrt{\alpha}l_0)$ is the Rice frequency [18,19]. This equation describes a parametrically driven oscillator which does not exhibit chaos. Due to the term with P^2 , $l(t)$ is parametrically driven by harmonic terms with frequencies 2ω , $2m\omega$ and $(m \pm 1)\omega$.

Equation (23) can be solved analytically by a perturbation theory that yields a hierarchy of linear equations which can be solved exactly order by order [19]. For $m=2$ the first order suffices; here $l(t)$ contains harmonics with the frequencies ω , 2ω , 3ω , and 4ω . The average soliton velocity is, due to Eq. (20),

$$\langle v \rangle = \langle \dot{X} \rangle = \frac{1}{T} \int_0^T \frac{P(t)l(t)}{M_0 l_0} dt, \quad (24)$$

which is nonzero because $l(t)$ contains harmonics which also appear in $P(t)$. In contrast to this, for $m=3$ there are only even harmonics in $l(t)$ which cannot resonate with the odd harmonics in $P(t)$. Therefore $\langle v \rangle$ vanishes, in agreement with the fact that the temporal shift symmetry is not broken for $m=3$ in Eq. (3).

Both $P(t)$ and $l(t)$ are continuous functions of the system parameters. Therefore $\langle v \rangle$ is continuous, too; there cannot be jumps, in contrast to the inhomogeneous ratchets with the “quantized” structure in Eq. (1).

V. HOMOGENEOUS RATCHETS: SIMULATIONS

Very recent simulations for sine-Gordon and ϕ^4 ratchets with biharmonic driving [19] demonstrated that the soliton dynamics is always regular, even for very small damping ($\beta=0.01$) and rather high driving frequencies ($\omega=0.1$ or $\omega=0.25$). In this paper we want to check whether this holds for even larger ω and for larger driving amplitudes. Moreover, we want to see to what extent the 2CC theory is still valid; this is an adiabatic theory which assumes that the driving force is weak and varies slowly such that the soliton is not deformed in a way which cannot be described approximately by the ansatz in Eq. (9).

We now use

$$f(t) = \frac{A_{\text{harm}}}{1 + a_r} [\sin(\omega t + \Theta_1) + a_r \sin(m\omega t + \Theta_2)] \quad (25)$$

as biharmonic driving force. Unlike Eq. (3), the above driving force can in some ways be directly compared to the harmonic driving force (5): If A_{harm} in Eq. (25) is chosen to be equal to A in Eq. (5), the total area enclosed between the time axis and the particular driving force is the same for both functions. Moreover, the maximum values of both functions are equal if A_{harm} and A are chosen as described above.

In the following we restrict ourselves to $m=2$, $\Theta_1=\Theta_2=0$ and $a_r=1$. Furthermore, we use the quantity A_{harm} to characterize the strength of the driving. Or, in terms of Eq. (3), $\epsilon_1=\epsilon_2=A_{\text{harm}}/2$ and $\delta_1=\delta_2=0$.

In Fig. 6(a) we see that for the biharmonic driving frequencies $\omega=0.38$, $m\omega=0.76$ and rather large driving amplitudes ($A_{\text{harm}}=0.3$) the 2CC theory still agrees with the simulations, if $\beta \geq 0.45$. Below this value, with decreasing β , the agreement becomes worse and worse, but the trajectories remain regular, both in the theory and in the simulations (see inset). For even stronger driving ($A_{\text{harm}}=0.6$) the soliton position can no longer be definitely determined for very small β [hatched region in Fig. 6(b)].

Finally we note that the above results only hold for continuous systems. The discrete sine-Gordon system with damping and biharmonic driving shows both regular and chaotic transport [36]. Moreover, $\langle v \rangle$ vs the driving amplitude exhibits a staircase structure as described in Eq. (1).

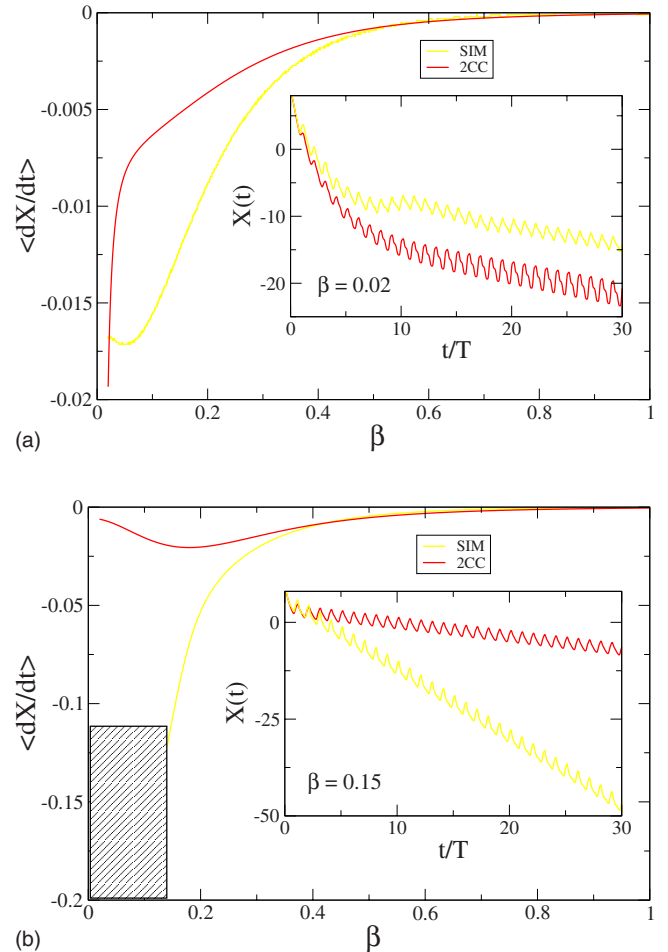


FIG. 6. (Color online) Mean soliton velocity $\langle v \rangle$ (average taken over 30 driving periods $2\pi/\omega$ after having waited for 30 periods) vs the damping coefficient β . The model parameters are $\omega=0.38$, $m=2$, $\Theta_1=\Theta_2=0$, and $A_{\text{harm}}=0.3$ (a) and 0.6 (b). The insets in both figures in each case show the soliton trajectories $X(t)$ for the smallest damping that was considered.

VI. CONCLUSIONS

We have demonstrated that sine-Gordon ratchets with strongly localized inhomogeneities, modeled by narrow high box functions, exhibit chaotic transport in certain regions of the parameter space. The reason is that the solitons behave as periodically driven particles in an effective, periodic, asymmetric potential; for such particle ratchet models chaotic transport is well known.

As a test for our prediction of chaotic transport, we suggest experiments on long Josephson junctions with strongly localized inhomogeneities. There are two types of such inhomogeneities, microshorts, and microresistors, which both have already been used in experiments. Our simulations, and also our CC theory, predict chaotic transport by solitons not only for very small damping, but also for certain other parameter regions [Fig. 2(a)]. Therefore there are good chances to find regions for which experiments can be performed.

In contrast to the inhomogeneous ratchets, homogeneous sine-Gordon ratchets with biharmonic driving, which breaks a time-shift symmetry, do not exhibit chaos. This can be

explained by a 2CC theory which eventually yields a decoupled linear ODE for the soliton momentum and a nonlinear ODE for the soliton width which can be understood as a parametrically driven oscillator. In fact, experiments with annular Josephson junctions, using biharmonic microwave driving, did not exhibit chaos.

The above 2-CC theory also explains that the mean soliton velocity is a smooth function of all the parameters of the model. In contrast to this, the mean soliton velocity in the inhomogeneous ratchets changes discontinuously as a function of the model parameters, which is well known for particle ratchet models.

ACKNOWLEDGMENTS

F.G.M. acknowledges the hospitality of the Theoretical Division and Center for Nonlinear Studies at Los Alamos National Laboratory. Work at Los Alamos was supported by USDOE. The authors thank A. Sánchez, Madrid, and R. Ecke, Los Alamos, for valuable advice.

APPENDIX

For the propagation of the solution $\phi(x, t)$ of Eq. (2) we use an explicit finite difference algorithm: After a spatial semidiscretization with stepsize $\Delta x=0.05$, the remaining coupled ODEs are solved using a fourth-order Runge-Kutta scheme with stepsize $\Delta t=0.01$. We use periodic boundary conditions. First of all we need the position of the soliton for every time step, that is, the soliton trajectories.

$$X(t) = x_n \quad \text{with} \quad \begin{cases} \phi(x_n, t) \geq (2m+1)\pi, \\ \phi(x_{n-1}, t) < (2m+1)\pi, \\ ([\phi(x_j, t) < (2m+1)\pi] \wedge \{\phi(x_j, t) > [2(m-1)+1]\pi\}) \forall j < (n-1), \\ ([\phi(x_j, t) > (2m+1)\pi] \wedge \{\phi(x_j, t) < [2(m+1)+1]\pi\}) \forall j > n. \end{cases} \quad (\text{A3})$$

If a perturbed sine-Gordon kink $\phi(x, t)$ does not fulfill Eq. (A3) for a certain time step, it is no longer possible to define meaningfully the position of its center $X(t)$. In this case there is no definite soliton trajectory $X(t)$ [white regions in Figs. 2 and 5, dark gray regions in Figs. 2(a), 2(b), and 5(a), hatched regions in Figs. 3, 4, and 6(b)].

2. Computation of the soliton velocity

Computing the soliton velocity $\dot{X}(t)$ using the discrete soliton positions

$$X(t_n = t_{\min} + n\Delta t)$$

may lead to severe discretization errors. Therefore we use a different approach: The area $\lambda = \int_{x_{\min}}^{x_{\max}} \phi[x, X(t), t] dx$ between the x axis and the kink $\phi(x, t = \text{const})$ depends linearly on the current soliton position $X(t)$ and vice versa:

1. Computation of the soliton position

For each time step

$$\phi_n(t) = \phi(x_n = x_{\min} + n\Delta x, t)$$

represents a perturbed sine-Gordon kink [Eq. (6)]. In case of free boundary conditions the position of the kink center $X(t)$ of an unperturbed sine-Gordon kink would be defined by

$$X(t) = x_n \quad \text{with} \quad \begin{cases} \phi(x_n, t) \geq \pi, \\ \phi(x_{n-1}, t) < \pi. \end{cases} \quad (\text{A1})$$

In case of periodic boundary conditions, a phase shift of 2π (soliton moves in the $-x$ direction) or -2π (soliton moves along the $+x$ direction) occurs every time the soliton switches from one side of the simulation region to the other. Hence the above definition has to be modified to

$$X(t) = x_n \quad \text{with} \quad \begin{cases} \phi(x_n, t) \geq (2m+1)\pi, \\ \phi(x_{n-1}, t) < (2m+1)\pi, \end{cases} \quad (\text{A2})$$

where $m=0, 1, \dots$, is an integer.

In the presence of (strong) perturbations, the above definitions are no longer sufficient. Consider for example a sine-Gordon kink with peaklike perturbations of height $\pm h_p$. If h_p is sufficiently large, a single kink $\phi(x, t = \text{const})$ may fulfill Eq. (A2) for different values of n and/or m at one and the same time. That is, one cannot specify a definite position of the kink center. Hence definition (A2) has to be modified again:

$$X[\lambda(t)] = m\lambda + \alpha. \quad (\text{A4})$$

For $X(t) = x_{\max}$, λ is approximately zero, for $X(t) = x_{\min}$, λ is approximately $2\pi(x_{\max} - x_{\min})$. Inserting these approximations in Eq. (A4) results in a set of coupled equations for m and α . Solving this set and reinserting the results into Eq. (A4) yields

$$\dot{X}[\lambda(t)] = x_{\max} - \frac{1}{2\pi}\lambda(t) = x_{\max} - \frac{1}{2\pi} \int_{x_{\min}}^{x_{\max}} \phi[x, X(t), t] dx \quad (\text{A5})$$

and, thus,

$$\dot{X}(t) = -\frac{1}{2\pi} \int_{x_{\min}}^{x_{\max}} \frac{\partial \phi[x, X(t), t]}{\partial t} dx, \quad (\text{A6})$$

where $\int_{x_{\min}}^{x_{\max}} \frac{\partial \phi[x, X(t), t]}{\partial t} dx$ is directly accessible during the computation.

3. Evaluation of soliton trajectories

To determine whether a soliton trajectory displays regular (n -periodic) or chaotic behavior [see Figs. 1(a) and 1(b), respectively], we apply methods of “symbolic dynamics.” The (possibly) complicated structure of the soliton trajectory $X(t)$ is translated into a sequence of simple symbols. This is done in a way that all needed information is conserved. On the other hand, all dispensable details are disregarded. The main problem is to find a “translation formula” satisfying the above claims.

Here we proceed as follows. The trajectory is examined on subsequent intervals

$$I_j = [t_w + jT; t_w + (j + 1)T],$$

with $j=0, 1, 2, \dots, m$ (t_w is a waiting time to exclude transients, $T = \frac{2\pi}{\omega}$ is the period of the driving force). On each of these intervals $X(t)$ is translated in one of the two symbols $\{1, 0\}$. For sinusoidal driving, the trajectory on every I_j is an oscillating function in time. We compute the distance

$$d_j = \max_{I_j}[X(t)] - \min_{I_j}[X(t)]$$

between the maximum and the minimum of $X(t)$ on I_j . If

$$d_{j+1} - d_j \geq \Delta,$$

$X(t)$ on I_j receives for example the symbol “1.” For

$$d_{j+1} - d_j < \Delta.$$

$X(t)$ on I_j is “translated” into “0.” The parameter Δ determines the “sensitivity” of the translation process. Good results are achieved by choosing Δ small compared to d . We always used $\Delta = 1/8$.

In the resulting sequence of symbols (length m), we search for repetitive structures. If a subsequence of symbols with length $n \in [1; \lfloor m/2 \rfloor]$ ($\lfloor \cdot \rfloor$ denotes the floor function) is repeated again and again, the corresponding trajectory shows regular, n -periodic behavior [light gray regions in Figs. 2(a) and 5(a)]. For $n > \lfloor m/2 \rfloor$, the corresponding trajectory displays chaotic soliton motion on the timescale given by the observation period $(m+1)T$ [white regions in Figs. 2(a) and 5(a)].

-
- [1] P. Hänggi and R. Bartussek, in *Nonlinear Physics of Complex Systems—Current Status and Future Trends*, edited by J. Parisi, S. C. Müller, and W. Zimmermann, Lecture Notes in Physics No. 476 (Springer, Berlin, 1996).
- [2] R. D. Astumian and P. Hänggi, *Phys. Today* **55**, 33 (2002).
- [3] F. Jülicher, A. Ajdari, and J. Prost, *Rev. Mod. Phys.* **69**, 1269 (1997).
- [4] P. Reimann, *Phys. Rep.* **361**, 57 (2002).
- [5] *Ratchets and Brownian Motors: Basics, Experiments and Applications*, edited by H. Linke [Appl. Phys. A: Mater. Sci. Process. **75**, 2 (2002)].
- [6] P. Jung, J. G. Kissner, and P. Hänggi, *Phys. Rev. Lett.* **76**, 3436 (1996).
- [7] J. L. Mateos, *Phys. Rev. Lett.* **84**, 258 (2000).
- [8] M. Barbi and M. Salerno, *Phys. Rev. E* **62**, 1988 (2000).
- [9] I. Zapata, R. Bartussek, F. Sols, and P. Hänggi, *Phys. Rev. Lett.* **77**, 2292 (1996).
- [10] F. Marchesoni, *Phys. Rev. Lett.* **77**, 2364 (1996).
- [11] F. Falo, P. J. Martínez, J. J. Mazo, and S. Cilla, *Europhys. Lett.* **45**, 700 (1999).
- [12] E. Trías, J. J. Mazo, F. Falo, and T. P. Orlando, *Phys. Rev. E* **61**, 2257 (2000).
- [13] M. Salerno and N. R. Quintero, *Phys. Rev. E* **65**, 025602(R) (2002).
- [14] G. Costantini, F. Marchesoni, and M. Borromeo, *Phys. Rev. E* **65**, 051103 (2002).
- [15] A. Gorbach, S. Denisov, and S. Flach, *Opt. Lett.* **31**, 1702 (2006).
- [16] S. Flach, Y. Zolotaryuk, A. E. Miroshnichenko, and M. V. Fistul, *Phys. Rev. Lett.* **88**, 184101 (2002).
- [17] M. Salerno and Y. Zolotaryuk, *Phys. Rev. E* **65**, 056603 (2002).
- [18] L. Morales-Molina, N. R. Quintero, F. G. Mertens, and A. Sánchez, *Phys. Rev. Lett.* **91**, 234102 (2003).
- [19] L. Morales-Molina, N. R. Quintero, A. Sánchez, and F. G. Mertens, *Chaos* **16**, 013117 (2006).
- [20] A. V. Ustinov, C. Coqui, A. Kemp, Y. Zolotaryuk, and M. Salerno, *Phys. Rev. Lett.* **93**, 087001 (2004).
- [21] L. Morales-Molina, F. G. Mertens, and A. Sánchez, *Eur. Phys. J. B* **37**, 79 (2004).
- [22] L. Morales-Molina, F. G. Mertens, and A. Sánchez, *Phys. Rev. E* **72**, 016612 (2005).
- [23] F. G. Mertens, L. Morales-Molina, A. R. Bishop, A. Sánchez, and P. Müller, *Phys. Rev. E* **74**, 066602 (2006).
- [24] L. Morales-Molina, F. G. Mertens, and A. Sánchez, *Phys. Rev. E* **73**, 046605 (2006).
- [25] A. V. Ustinov, *Phys. Lett. A* **136**, 155 (1989).
- [26] N. R. Quintero, B. Sánchez-Rey, and M. Salerno, *Phys. Rev. E* **72**, 016610 (2005).
- [27] M. Barbi and M. Salerno, *Phys. Rev. E* **63**, 066212 (2001).
- [28] C. R. Willis and M. Farzaneh, *Phys. Rev. E* **69**, 056612 (2004).
- [29] F. G. Mertens, H. J. Schnitzer, and A. R. Bishop, *Phys. Rev. B* **56**, 2510 (1997).
- [30] M. J. Rice and E. J. Mele, *Solid State Commun.* **35**, 487 (1980); M. J. Rice, *Phys. Rev. B* **28**, 3587 (1983).
- [31] N. R. Quintero, A. Sánchez, and F. G. Mertens, *Phys. Rev. Lett.* **84**, 871 (2000).
- [32] N. R. Quintero, A. Sánchez, and F. G. Mertens, *Phys. Rev. E* **62**, 5695 (2000).
- [33] A. R. Bishop, K. Fesser, P. S. Lomdahl, and S. E. Trullinger, *Physica D* **7**, 259 (1983).
- [34] N. R. Quintero, A. Sánchez, and F. G. Mertens, *Eur. Phys. J. B* **16**, 361 (2000).
- [35] N. R. Quintero, B. Sánchez-Rey, and J. Casado-Pascual, *Phys. Rev. E* **71**, 058601 (2005).
- [36] Y. Zolotaryuk and M. Salerno, *Phys. Rev. E* **73**, 066621 (2006).